Effects of phase and coupling between the vibrational modes on selective excitation in coherent anti-Stokes Raman scattering microscopy

Vishesha Patel, Vladimir S. Malinovsky, and Svetlana Malinovskaya
Department of Physics and Engineering Physics, Stevens Institute of Technology, Hoboken, New Jersey 07030, USA
(Received 14 October 2009; revised manuscript received 24 February 2010; published 8 June 2010)

Coherent anti-Stokes Raman scattering (CARS) microscopy has been a major tool of investigation of biological structures as it contains the vibrational signature of molecules. A quantum control method based on chirped pulse adiabatic passage was recently proposed for selective excitation of a predetermined vibrational mode in CARS microscopy [Malinovskaya and Malinovsky, Opt. Lett. **32**, 707 (2007)]. The method utilizes the chirp sign variation at the peak pulse amplitude and gives a robust adiabatic excitation of the desired vibrational mode. Using this method, we investigate the impact of coupling between vibrational modes in molecules on controllability of excitation of the CARS signal. We analyze two models of two *coupled* two-level systems (TLSs) having slightly different transitional frequencies. The first model, featuring degenerate ground states of the TLSs, gives robust adiabatic excitation and maximum coherence in the resonant TLS for positive value of the chirp. In the second model, implying nondegenerate ground states in the TLSs, a population distribution is observed in both TLSs, resulting in a lack of selectivity of excitation and low coherence. It is shown that the relative phase and coupling between the TLSs play an important role in optimizing coherence in the desired vibrational mode and suppressing unwanted transitions in CARS microscopy.

DOI: 10.1103/PhysRevA.81.063404 PACS number(s): 32.80.Qk, 42.50.Hz, 42.65.Dr

I. INTRODUCTION

In the past decade, coherent anti-Stokes Raman scattering (CARS) has developed as a promising technique for imaging of various biological species (e.g., living cells and cancerous cells) and also for combustion diagnostics and monitoring of molecules. The recent advances in shaping of ultrafast femtosecond laser pulses [1] along with demonstration of different experimental and theoretical techniques [2–14] of steering a system to the desired quantum yield has made CARS a major tool of investigation of biological structures. Experimental configurations such as box-CARS [15], frequency modulation CARS (FM-CARS) [16], backward direction (EPI-CARS) [17], heterodyne CARS [18], polarization-CARS [19], Fourier-transform CARS (FT-CARS) [20], and interferometric CARS [21] are among the most promising ones. A major drawback of the CARS technique is the nonresonant background signal. Implementation of the femtosecond pulses in combination with the quantum control methods makes it possible to selectively drive a predetermined Raman transition and effectively suppress the background signal. It has been shown recently [22] that an application of two femtosecond chirped laser pulses induces adiabatic passage in a system, resulting in maximum coherence in a selected vibrational mode and in turn providing an optimal CARS signal. In this paper we analyze the impact of the coupling between Raman active vibrational modes on selectivity of their excitation in CARS microscopy using the method proposed in [22]. We study two theoretical models demonstrating control over the quantum yield and optimization of the CARS signal. Each model consists of two effective two-level systems (TLSs) with (a) degenerate ground states and (b) nondegenerate ground states, which interact with two chirped femtosecond pulses within the Raman configuration in accordance with [22]. The first model with degenerate lower states may be used to describe the induced dipole moments coupled via dipole-dipole interactions and subject to interaction with external electromagnetic fields [23], while second one with nondegenerate lower states is useful for the description of Raman modes present in a molecule and interacting with light [12].

The nonlinear nature of CARS is due to four-wave mixing. When the frequency difference between the pump and Stokes beams is in resonance with a molecular vibration, it excites the molecule to the higher vibrational level, creating a coherence of the corresponding transition. On de-excitation by the probe pulse anti-Stokes frequency light is emitted. It contains the vibrational signature of the molecule, which has a unique nature. Thus, rich information can be extracted from the CARS spectrum. By applying femtosecond chirped laser pulses as in [22] within two models, and performing relative phase dependence studies, we analyze the role of coupling between vibrational modes as well as relative phase dependence on optimizing the coherence in the desired vibrational mode and suppressing the unwanted one. We would like to point out that our results are related to the so-called strong-field control regime in which perturbation theory with respect to the external field amplitude is not valid and the exact solution of the Schrödinger equation must be applied to describe excitation dynamics correctly. Note also that only in the strong-field regime can 50:50 coherent superposition of states be created to generate the maximum CARS signal.

In Sec. II we present a general theoretical approach for the description of TLSs interaction with the pump and Stokes pulses within the Raman configuration. In Sec. III the numerical results are presented for the degenerate model (III A) and for the nondegenerate model (III B) obtained from the solution of the time-dependent Schrödinger equation and the dressed state analysis. In Sec. IV the results are summarized.

II. THEORY

We consider a semiclassical model of light-matter interaction, where strong femtosecond laser pulses interact with two coupled TLSs representing two Raman-active vibrational

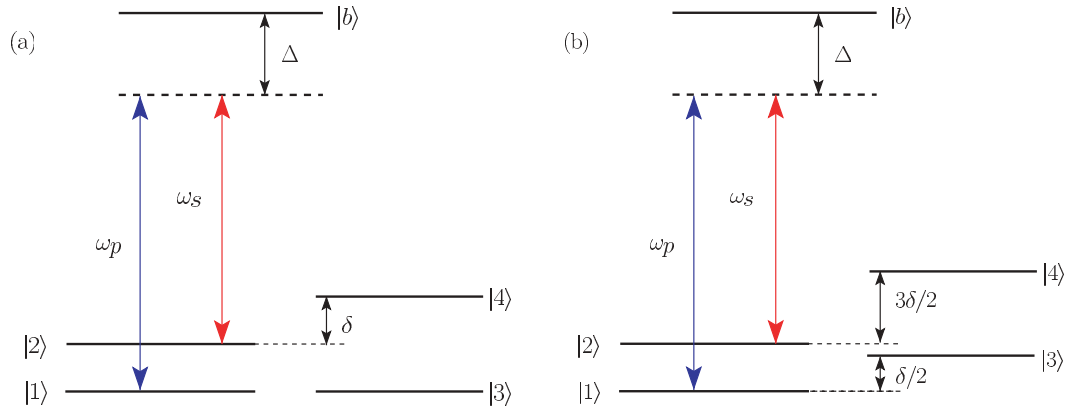

FIG. 1. (Color online) Schematic of the energy levels in the degenerate model (a) and nondegenerate model (b).

modes in a molecule. A molecular medium of interest may be considered as an ensemble of TLSs [2,22], with no relaxation or collisional dephasing effects taken into account. We investigate two models: one with degenerate ground states [Fig. 1(a)] and another with nondegenerate ground states [Fig. 1(b)]. Here the $|1\rangle - |2\rangle$ TLS has transition frequency ω_{21} and the $|3\rangle - |4\rangle$ TLS has transition frequency ω_{43}. These two modes are coupled by an external field, meaning that all states are effectively coupled. In addition, we take into account the phase relation between different modes, assuming that the relative phase between initially populated states $|1\rangle$ and $|3\rangle$ is random in a large ensemble of molecules. Therefore, most of the presented results are phase-averaged. Note that the bandwidth of the applied pulses is larger than the frequency mode difference. Our goal is to suppress coherence in the $|3\rangle - |4\rangle$ TLS and to create maximum coherence in the $|1\rangle - |2\rangle$ TLS. The maximum coherence is the condition for the optimal CARS signal for given pulse intensity, according to the Maxwell-Bloch equations. The frequency chirped pump and Stokes pulses having central frequencies ω_p and ω_s are defined as

$$E_{p,s}(t) = E_{p0,s0}(t)\cos[\omega_{p,s}(t-t_0) + \alpha_{p,s}(t-t_0)^2/2],$$
$$E_{p0,s0}(t) = \frac{E_0}{\left(1+\alpha'^2_{p,s}/\tau_0^4\right)^{1/4}}\exp[-(t-t_0)^2/2\tau^2], \quad (1)$$

where $E_{p0}(t)$ and $E_{s0}(t)$ are the time-dependent pump and Stokes field envelopes, $\alpha_{p,s}$ and $\alpha'_{p,s}$ are the linear temporal and spectral chirps of the pump and Stokes pulse, respectively, and $\tau_{p,s} = \tau_0^2\sqrt{1+\alpha'^2_{p,s}/\tau_0^4}$ is the chirp-dependent pulse duration. For zero chirp, frequency difference $\omega_p - \omega_s$ is in resonance with the frequency ω_{21}, and the pump and Stokes pulse duration before chirping is τ_0.

Interaction of vibrational modes with ultrafast chirped laser pulses is described in the rotating wave approximation by a semiclassical Hamiltonian obtained using adiabatic elimination of the virtual state $|b\rangle$. Within the field interaction representation the Hamiltonian for the degenerate model reads

$$H = \begin{pmatrix} -d(t)-\Omega_d(t) & -\Omega_3(t) & -\Omega_1(t) & -\Omega_3(t) \\ -\Omega_3(t) & d(t)+\Omega_d(t) & -\Omega_3(t) & -\Omega_2(t) \\ -\Omega_1(t) & -\Omega_3(t) & -d(t)-\Omega_d(t) & -\Omega_3(t) \\ -\Omega_3(t) & -\Omega_2(t) & -\Omega_3(t) & \delta+d(t)+\Omega_d(t) \end{pmatrix}. \quad (2)$$

The interaction Hamiltonian for the nondegenerate model reads

$$H = \begin{pmatrix} -d(t)-\Omega_d(t) & -\Omega_3(t) & -\Omega_1(t) & -\Omega_3(t) \\ -\Omega_3(t) & d(t)+\Omega_d(t) & -\Omega_3(t) & -\Omega_2(t) \\ -\Omega_1(t) & -\Omega_3(t) & \delta/2-d(t)-\Omega_d(t) & -\Omega_3(t) \\ -\Omega_3(t) & -\Omega_2(t) & -\Omega_3(t) & 3\delta/2+d(t)+\Omega_d(t) \end{pmatrix}. \quad (3)$$

Here $d(t) = (\alpha_s - \alpha_p)(t-t_0)/2$, $\Omega_d(t) = [\Omega_1(t) - \Omega_2(t)]/2$, $\Omega_{1,2}(t) = \mu^2 E^2_{p0,s0}(t)/(4\hbar^2\Delta)$ are the ac Stark shifts originated from the two-photon transitions, $\mu \equiv \mu_{ij}$ is the dipole moment (for simplicity we consider all the dipole moments to be equal to 1 Debye), Δ is the single photon detuning from the excited state $|b\rangle$ (assumed equal for both pump and Stokes pulse frequencies), and $\Omega_3(t) = \mu^2 E_{p0}(t)E_{s0}(t)/(4\hbar^2\Delta)$ is the effective Rabi frequency. The diagonal elements of the Hamiltonian describe bare state energies in the field interaction representation; they depend on the chirp parameters $\alpha_{p,s}$ and detunning $\delta = \omega_{43} - \omega_{21}$. The off-diagonal elements represent coupling of the bare

states through the effective Rabi frequency and the ac Stark shifts.

Here we consider the case when pump and Stokes chirp rates have equal value, $|\alpha_p| = |\alpha_s| = \alpha$. The control in the TLSs is achieved by linearly chirped pulses with chirp parameters such that the frequency difference of the pump and Stokes pulses first reduces at a 2α rate and comes to resonance with ω_{21} at the central time t_0 without further change till the end of the pulse. This method is known as the roof method [22]. In the case of two uncoupled TLSs, studied in [22], the proposed scheme resulted in the creation of maximum coherence in the resonant TLS and zero coherence in the off-resonant TLS. Now, the model is modified by switching on the coupling between two TLSs via an external fields in order to analyze the impact of the coupling on controllability of excitation and also the attendant relative phase effects.

III. NUMERICAL RESULTS AND DISCUSSION

To analyze the dynamics of the population and coherence we solve the time-dependent Schrödinger equation with the Hamiltonians in Eqs. (2) and (3) for the total wave function $|\Psi(t)\rangle = \sum_{i=1}^{4} a_i(t)|i\rangle$, where $a_i(t)$ are the time-dependent probability amplitudes. Calculations were performed using the Runge-Kutta method [24] under the initial conditions of equally populated ground states, $|1\rangle$ and $|3\rangle$, which is likely to be the case for molecules at room temperature. The population of each state was chosen to be 0.5, giving the total population in the system equal to unity and coherence value ranging from zero to a maximum value of 0.5. In the following we are using standard density matrix notation for the population $\rho_{ii} = |a_i(t)|^2$ and coherence $\rho_{ij} = |a_i^*(t)a_j(t)|, i,j = 1,2,3,4$. The parameters of the fields and the systems used in numerical calculations correlate with experimental conditions discussed in [9,25] and also used in [11]. They are also an equally good fit to address different vibrational modes of CH_n molecular species in biological samples [17]. We chose $\omega_{21} = 84.9$ THz (2840 cm^{-1}) and $\omega_{43} = 87.6$ THz (2930 cm^{-1}). The range of intensity of the laser fields is from 10^{11} to 10^{13} W/cm^2, and the transform-limited pulse duration is $\tau_0 = 176$ fs. The spectral chirps used in the calculations are $\alpha'_{p,s} = 31 \times 10^{-5}$ cm^{-2}, giving a chirped pulse duration $\tau = 1.8$ ps.

Let us discuss phase averaging in detail to gain more understanding of its importance in making a connection with an experimentally measurable CARS signal. Phase is embedded as the complex part in the probability amplitude of the state. When states are coupled by external fields, the relative phase between them just before the fields strike the medium is of key importance since it determines the evolution of the population and coherence in the TLSs. Obviously, the quantum yield at the end of the pulse is phase dependent. One can prepare a particular relative phase between initially populated states by optical pumping [26] into state $|1\rangle$ and creating a $|1\rangle - |3\rangle$ state coherence using a Raman scheme. Some values of the initial relative phase are known to bring the system to an optimal quantum yield [27]. In the bulk gas or liquid medium, molecules have all possible relative phases between vibrational states at the instant when pulses strike the molecular medium. The Raman signal measured form such a macroscopic ensemble of molecules is phase-averaged. To include this idea in our theoretical approach, we take into account the effect of relative phase between initially populated states by performing phase averaging. The procedure consists of calculating state physical quantities at the end of the pulse for 100 initial relative phases between initially populated states $|1\rangle$ and $|3\rangle$ ranging from zero to 2π and averaging over the results obtained.

A. Degenerate model

The coherence density plots of the resonant and detuned systems are depicted in Fig. 2 as a function of effective pulse area $A = \int \Omega_3(t)dt$ and dimensionless frequency chirp parameter α'/τ_0^2. The sign of the chirp parameter, α', determines the direction of the pump chirp before the central time when the sign changes. The Stokes chirp is the linear chirp and it has opposite sign to the pump chirp before the central time. The transform-limited pulse duration is $\tau_0 = 15[\omega^{-1}]$, where ω is the unit frequency equal to ω_{21}. This value of τ_0 corresponds to 176 fs. The figure shows that there is a broad parameter region providing maximum coherence ρ_{12} in the resonant TLS (shown in blue) for the positive chirp values. In the off-resonant TLS, coherence is zero in the same region of field parameters. Negative values of the chirp parameter do not provide selective excitation of coherence in

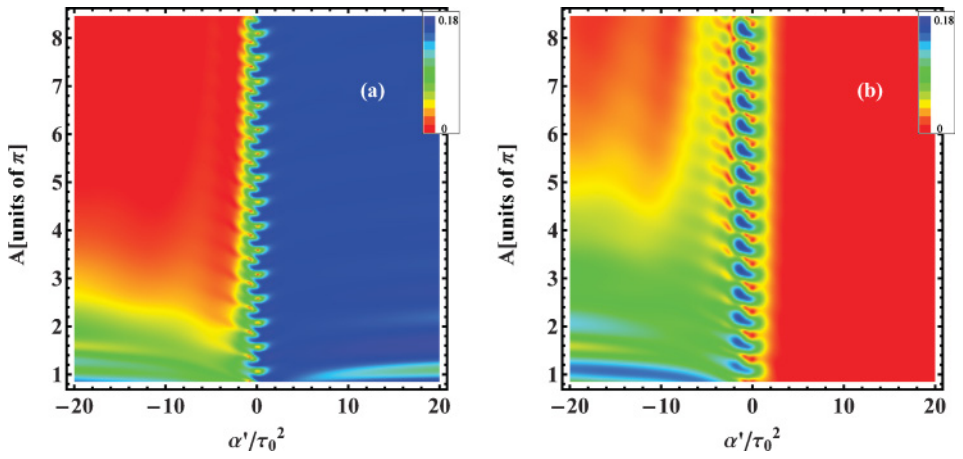

FIG. 2. (Color online) Degenerate model: Density plot of averaged coherence for the resonant (a) and off-resonant (b) systems as a function of the effective pulse area, A, and chirp parameter, α'/τ_0^2.

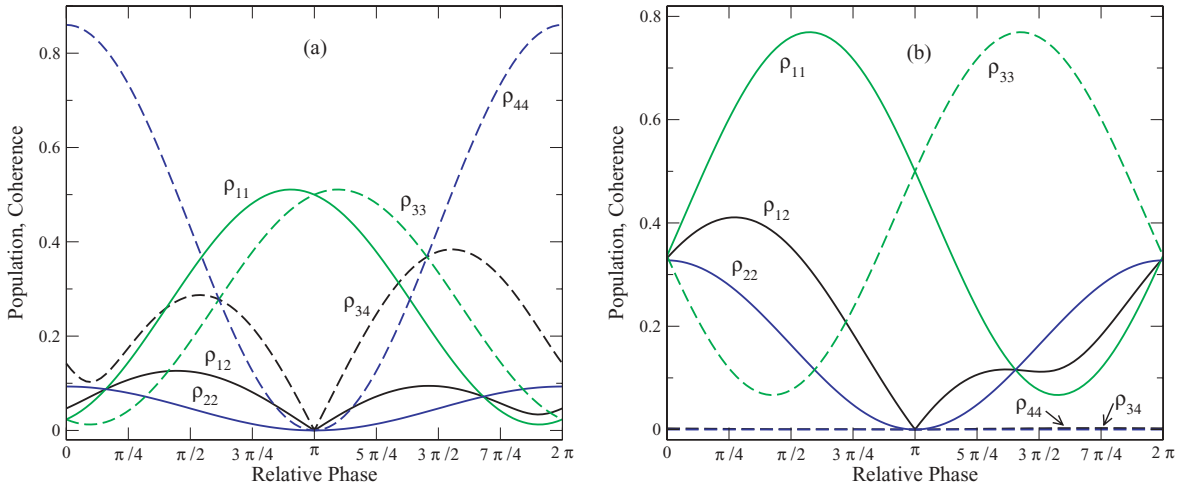

FIG. 3. (Color online) Degenerate model: Relative phase dependence of population, ρ_{ii}, and coherence, ρ_{ij}, at final time for positive (a) and negative (b) chirp of the Stokes pulse; $\Omega_3(t_0) = 0.35[\omega_{21}]$ (respective effective pulse area $A \simeq 2.95\pi$); $|\alpha'|/\tau_0^2 = 10$.

the coupled TLSs. Note that the effective pulse area of 0.85π (corresponding to the chirped pulse peak intensity in the range of 10^{11} W/cm^2) shows coherent control of the vibrational excitations in molecules. This is a useful addition to previously obtained results on selective excitation in a strong-field regime when the field intensity ranges from 10^{12} to 10^{13} W/cm^2 [22]. Thus, the chirped pulse adiabatic passage method—the roof method—is feasible in achieving maximum coherence in a predetermined vibrational mode in the presence of strong coupling between many Raman-active vibrational modes via external fields.

Understanding the mechanism of selective excitation under the condition of the coupling between vibrational modes is gained through the analysis of the dressed state picture. We refer in this case only to a particular value of the initial relative phase. To do so, we first consider the dependence of coherence and population on the initial relative phase between the ground states $|1\rangle$ and $|3\rangle$ at the final time, which is shown in Fig. 3. In the case of negative Stokes chirp [Fig. 3(b)], for most values of the relative phase between 0 to 2π, there is a strong coherence in the resonant TLS, while there is zero coherence in the nonresonant TLS. The relative phase π can be inferred as the one creating the dark state, as the coherences ρ_{12} and ρ_{34} both go to zero and the entire population is collected in the ground states of TLSs, meaning that the TLSs stay uncoupled from the external fields. In the case of positive Stokes chirp [Fig. 3(a)], both coherences ρ_{12} and ρ_{34} have some value and the relative phase dependence is almost symmetrical with respect to phase π, so that averaging over the phase gives almost zero, as shown in Fig. 2 [see the left side of plots (a) and (b)]. The asymmetry in the coherence value at the final time with respect to the chirping direction (positive or negative) might be clearly observed by using the dressed states. As usual, the dressed states can be obtained by diagonalizing the 4×4 Hamiltonians [Eq. (2) or (3)] by solving the corresponding eigenvalue problem. In the present situation, the expressions for the dressed state energies and corresponding dressed vectors are too complicated to be presented in a compact form here. In general, each dressed state is a linear superposition of all four bare states, $|i\rangle$, with coefficients depending on the Rabi frequency, detuning, and pulse chirps. The energies of the dressed states are shown in Fig. 4.

Within the adiabatic approximation, the system dynamics starts in dressed state I and III, which initially correlates with the bare states $|1\rangle$ and $|3\rangle$, correspondingly, independently from the chirping direction. Consider first positive Stokes chirp [Fig. 4(a)]. As time evolves and the pulse intensity increases, dressed state III reaches the region of avoiding

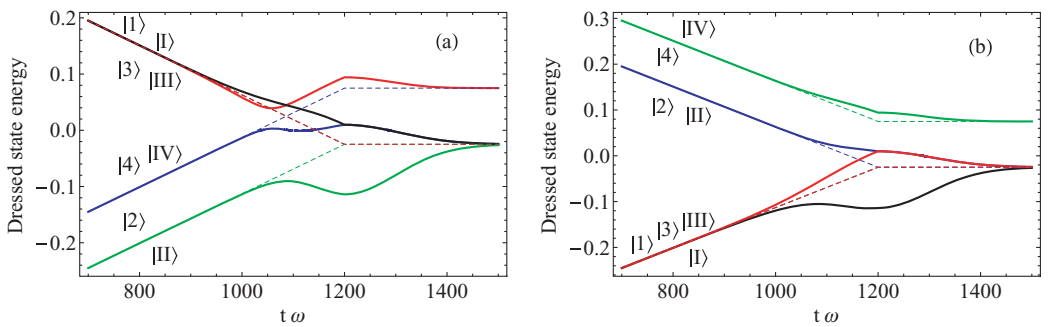

FIG. 4. (Color online) Degenerate model: Dressed state energies (solid lines) and bare state energies (dashed lines) as a function of time for the positive (a) and negative (b) Stokes chirp; $\Omega_3(t_0) = 0.35$ (respective effective pulse area $A \simeq 2.95\pi$); $|\alpha'|/\tau_0^2 = 10$.

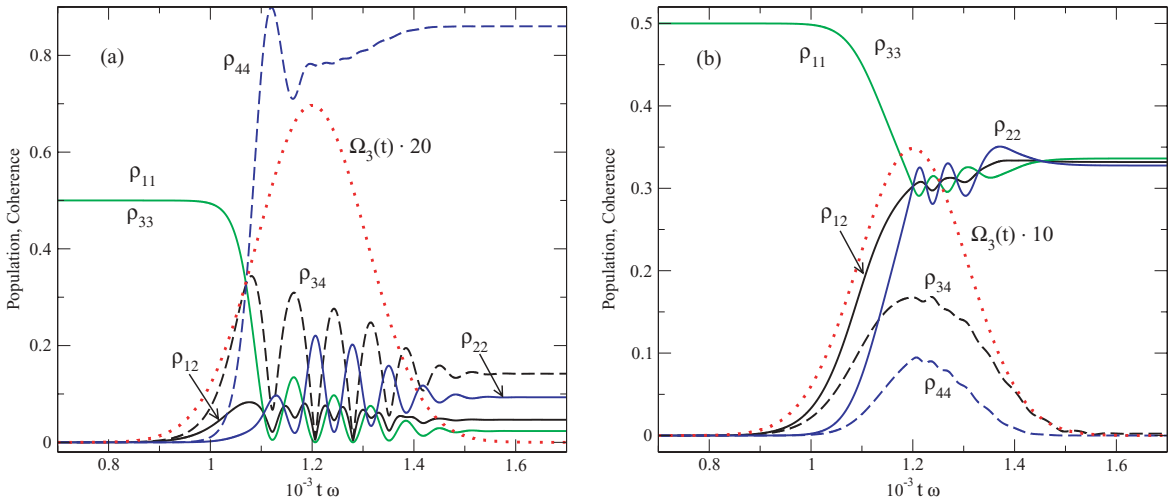

FIG. 5. (Color online) Degenerate model: Coherences and state populations as a function of time for the positive (a) and negative (b) Stokes chirp; $\Omega_3(t_0) = 0.35[\omega_{21}]$ (respective effective pulse area $A \simeq 2.95\pi$); $|\alpha'|/\tau_0^2 = 10$.

crossing with dressed state IV, followed immediately after that by diabatic crossing with state I. It is clear that in the adiabatic approximation t dressed state III correlates with state $|4\rangle$ at the final time and will provide population transfer to this bare state. Dressed state I has several diabatic crossings with states III and IV and it correlates with state $|1\rangle$ at a later time. In fact, dressed states I, II, and IV coincide in energy at a later time; therefore (if we follow this route), the system will end up in a coherent superposition of all three bare states, $|1\rangle$,$|2\rangle$, and $|3\rangle$, at the final time. The population of the state $|3\rangle$ at the final time depends strongly on the adiabaticity of the first avoided crossing between the dressed states III and IV: The higher the adiabaticity parameter the less population will be in state $|3\rangle$ at the end.

For negative Stokes chirp [Fig. 4(b)], the dressed state energies are much different. Now, dressed state I effectively has only one avoided crossing at a central time and it is located far below all the other dressed states. In the adiabatic approximation the wave function dynamics of states $1\rangle$ and $|2\rangle$ is very close to the case of the two-level system considered in [22]. This is the most robust solution, which is supported by the results presented in Fig. 2 [see the right side of panel (a)], where maximum coherence in the resonant mode can be prepared over a wide range of the chirp rate and pulse area. Of course, averaging over the relative phase reduces the maximum value of the coherence.

Figure 5 shows the dynamics of the state population and coherence as a function of time for zero initial relative phase between states $|1\rangle$ and $|3\rangle$. In essence, this figure confirms the discussion of the dressed state analysis presented here. For positive Stokes chirp [Fig. 5(a)], the population is mostly transferred to state $|4\rangle$ due to adiabatic following in dressed state III, which correlates with the bare state $|4\rangle$ [Fig. 3(a)]. At the final time the coherences ρ_{12} and ρ_{34} are of order 0.05. For negative Stokes chirp [Fig. 5(b)], population dynamics follows the dressed state picture presented in Fig. 3(a). At the final time state $|4\rangle$ is empty and the whole population is almost equally distributed among states $|1\rangle$, $|2\rangle$, and $|3\rangle$, which gives maximum coherence for the resonant mode ($\rho_{12} \approx 0.33$). The result additionally demonstrates a good correlation between the dressed state picture and the exact solution, showing that by preparing a molecular system in an initial state with a particular relative phase between vibrational modes we can achieve a high value of coherence for the resonant mode and zero excitation in the off-resonant mode.

From this discussion it follows that there is a near-adiabatic solution for achieving maximum coherence in a predetermined

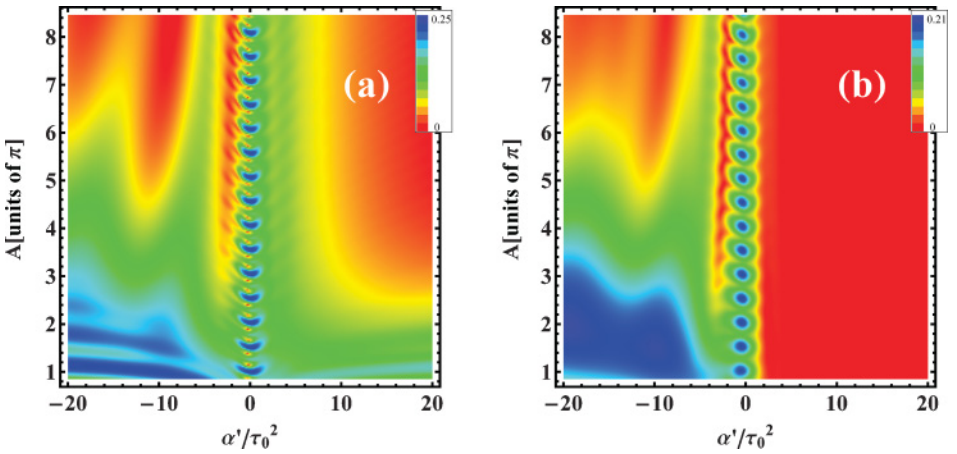

FIG. 6. (Color online) Nondegenerate model: Density plot of averaged coherence for the resonant (a) and off-resonant (b) systems as a function of the effective pulse area, A, and chirp parameter, α'/τ_0^2.

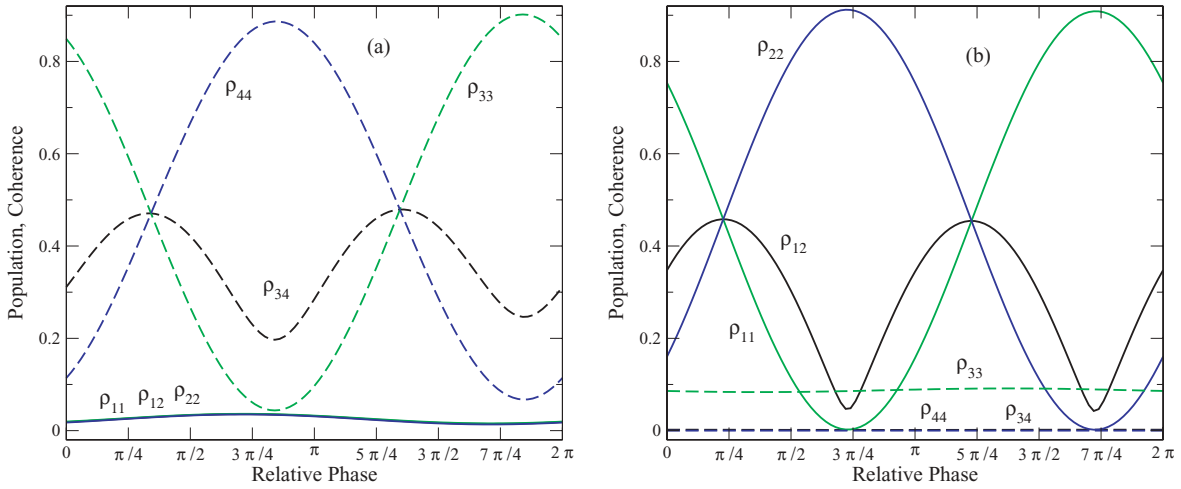

FIG. 7. (Color online) Nondegenerate model: Relative phase dependence of population, ρ_{ii}, and coherence, ρ_{ij}, at final time for positive (a) and negative (b) chirp of the Stokes pulse; $\Omega_3(t_0) = 0.7[\omega_{21}]$ (respective effective pulse area $A \simeq 5.9\pi$); $|\alpha'|/\tau_0^2 = 10$.

TLS in the presence of its coupling with another TLS via external fields. This solution may be achieved in a relatively strong field regime. The results demonstrate that coherence in both modes is sensitive to the initial relative phase between originally populated states and to the field parameters such as intensity and the chirp sign.

B. Nondegenrate model

In this section we discuss the nondegenerate model in which the ground states $|1\rangle$ and $|3\rangle$ are shifted by $\delta/2$ [Fig. 1(b)]. The dynamics of the system is governed by the time-dependent Schrödinger equation with the Hamiltonian in Eq. (3). Figure 6 shows the density plots of phase-averaged coherence ρ_{12} and ρ_{34} as a function of the chirp parameter and effective pulse area. The range of the effective pulse area corresponds to the peak intensity of a transform-limited pulse in the range of 32×10^{11} to 32×10^{12} W/cm^2. The chirp parameter spans $\alpha'/\tau_0^2 = \pm 20$, corresponding to $\pm 62 \times 10^{-5}$ cm^{-2}.

Here, essentially for both coherences ρ_{12} and ρ_{34}, the region of positive chirp (of the pump pulse before the central time) shows zero value in strong fields, where one could expect adiabatic solution. However, there is a relatively large area of the moderate chirp rates which provides ρ_{12} coherence of order 0.15 [green area in Fig. 6(a), left side] while ρ_{34} is almost zero [Fig. 6(b), left side]. In the negative chirp region the topology of the coherence density plots are almost identical, meaning that there is no selectivity of the mode excitation.

It is clear that there is a dependence of the coherence on the initial relative phase between states and that a specific relative phase may provide the time evolution leading to maximum coherence in the $|1\rangle - |2\rangle$ TLS and zero coherence in the $|3\rangle - |4\rangle$ TLS. The phase dependence of ρ_{12} and ρ_{34} at the final time is demonstrated in Fig. 7. Notably, coherence ρ_{12} is nonzero and significant while coherence ρ_{34} is negligible for any relative initial phase in the case of negative Stokes chirp [Fig. 7(b)]. The positive Stokes chirp case shows relatively high values of the ρ_{34} coherence while ρ_{12} is very small [Fig. 7(a)].

Let us discuss the case of zero relative phase in more detail. Figure 8 presents the density plots of ρ_{12} and ρ_{34} as a function of effective pulse area and the spectral chirp parameter when the initial relative phase is zero. Note that the field conditions are the same as in Fig. 6. Blue regions of maximum coherence ρ_{12} and red regions of zero coherence ρ_{34} are observed for both positive and negative chirp. It is interesting that the selectivity of excitation of TLSs resulting in optimal values of coherence is achieved for zero relative

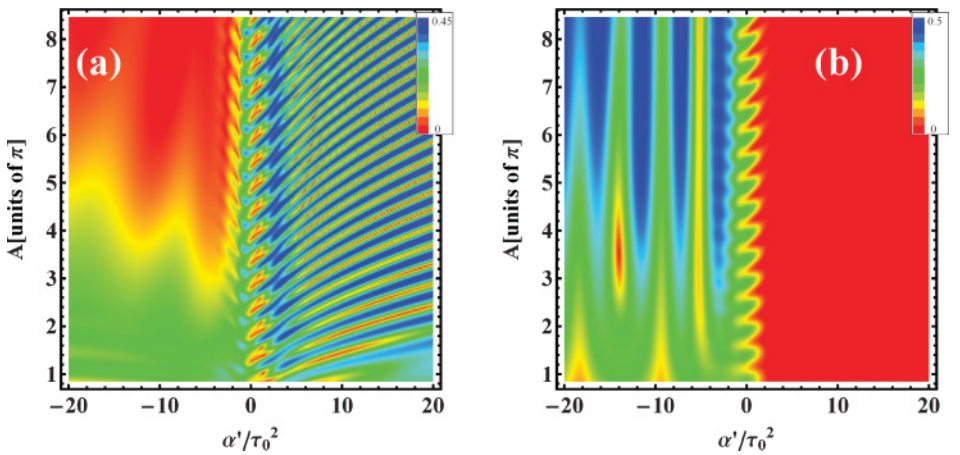

FIG. 8. (Color online) Nondegenerate model: Density plot of coherence for the resonant (a) and off-resonant (b) systems as a function of the effective pulse area, A, and chirp parameter, α'/τ_0^2, for zero initial relative phase between states $|1\rangle$ and $|3\rangle$.

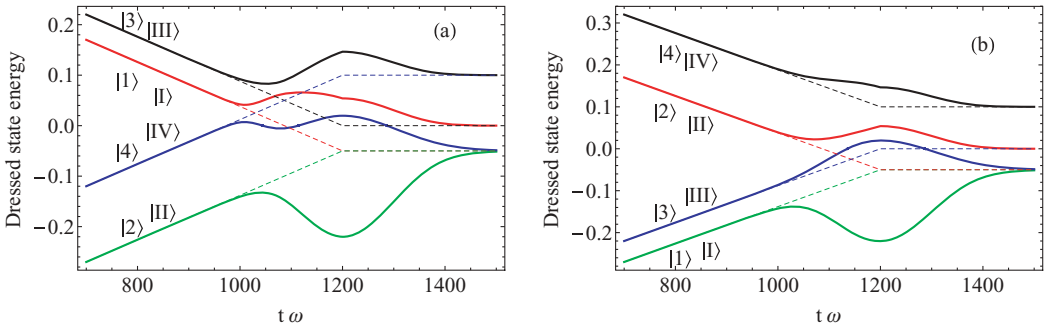

FIG. 9. (Color online) Nondegenerate model: Dressed state energies (solid lines) and bare state energies (dashed lines) as a function of time for the positive (a) and negative (b) Stokes chirp; $\Omega_3(t_0) = 0.7$ (respective effective pulse area $A \simeq 5.9\pi$); $|\alpha'|/\tau_0^2 = 10$.

phase in a relatively weak field regime (0.85π pulse area). This is an important observation that highlights the coupling as an additional channel of controllability. In [22], where a model of two uncoupled TLSs was investigated, it was demonstrated that no selectivity can be achieved in the weak-field regime. However, when coupling between TLSs is present, it opens an additional channel for population transfer and, depending on the initial phase conditions, leads to the desired selective excitation with optimal values of coherences ρ_{12} and ρ_{34} in the moderate fields.

To see the adiabatic effects of light-matter interaction within the current model, we analyzed the dressed state picture. We numerically diagonalized the Hamiltonian in Eq. (3) and obtained the time-dependent energy of the dressed states and eigenvectors. The diagonalization was carried out under the conditions that (a) the ac Stark shifts are equal, $\Omega_1(t) = \Omega_2(t)$, due to identical pulse envelopes of the pump and Stokes pulses, and (b) the chirp parameter α_p changes sign at the central time, t_0, while the absolute value of the pump and Stokes pulse chirps is preserved. Figure 9 shows the dressed state energies (solid lines) and the bare states energies (dashed lines) as a function of time.

For the case of positive Stokes chirp three dressed states are involved in the time evolution of the system: dressed states I, III, and IV. Initially, dressed states I and III are populated by an initial population of bare states $|1\rangle$ and $|3\rangle$. As time evolves, dressed states I and IV approach, avoiding crossing, followed by the avoided crossing between states I and III. These two avoided crossings are not really separated in time, and most probably they cannot be treated independently. This complex situation results in essentially nonadiabatic population transfer among dressed states I, III, and IV. In turn, populations and coherences in the bare state basis show no sign of adiabatic control. However, there are areas of the parameters [blue area in Fig. 8(b), left side] where $\rho_{34} = 0.5$, which means that the whole population is now distributed between states $|3\rangle$ and $|4\rangle$. In the dressed state these regions correspond to the case when only two dressed states I and III are populated, and the first avoided crossing between I and IV is adiabatic; at later time state I correlates with bare state $|3\rangle$ while dressed state III correlates with bare state $|4\rangle$.

In the case of negative Stokes chirp [Fig. 9(b)], the dressed state picture looks much better for realizing adiabatic control at least of the resonant mode. Here dressed states I, II, and III are involved in the system dynamics and dressed state I is well separated from all other states. However, there is the avoided crossing between states III and II which effectively involves bare state $|3\rangle$ in evolution. In fact, the oscillations in the coherence ρ_{12} at the final time [Fig. 8(a), left side] as a function of the effective pulse area at the fixed chirp rate demonstrate the importance of the dynamical phase, meaning that several dressed states provide a contribution to the bare state populations; in this case they are the states I, II, and III. Note that at some values of the effective pulse area the population is only in states $|1\rangle$ and $|2\rangle$, which provide $\rho_{12} = 0.5$ at the fixed relative phase.

IV. CONCLUSION

We investigated the impact of the coupling between Raman-active vibrational modes on the controllability of their excitation. We also analyzed a possibility for optimizing the CARS signal in the case of coupled Raman-active vibrational modes for enhanced imaging. The use of a chirped pump and Stokes laser pulses in CARS allows one to achieve selective excitation in a predetermined vibrational mode, within which many of these excitations have close transitional frequencies. A theory developed in this paper implements the roof method [22] to a system of two *coupled* TLSs and gives us a broader essence of the method implementation in the laboratory. The use of femtosecond chirped laser pulses with chirp sign variation at a central time provides adiabatic or near-adiabatic passage in two coupled TLSs, leading to significant coherence in the resonant TLS and zero coherence in nonresonant TLS in the presence of coupling between them via external electric fields. The results show that by applying the roof method one can stay in the low-intensity regime and gain coherent control over the system. The positive chirp is desirable for the excitation in the resonant TLS for the degenerate model. Also, single-phase calculations support this idea for optimizing coherence among the states of interest. For the nondegenerate model, the phase-averaged solution gives population transfer among all states in TLSs. Near-adiabatic passage resulting in substantial coherence in the resonant mode is observed for a single, fixed phase between initially populated states in the coupled TLSs. The analysis of dressed states supports this conclusion by showing an optimal population transfer between the ground and excited states in the resonant TLS, which is a desirable condition to have a high value of coherence. Thus, the roof method can be used for noninvasive imaging

of biological specimens in the presence of coupling between vibrational modes and can be an efficient tool to suppress the contribution of the nonresonant background and, thus, improve the selectivity and chemical sensitivity of the CARS signals.

ACKNOWLEDGMENT

This work is supported by the National Science Foundation under Grant No. PHY-0855391.

[1] F. He, H. S. S. Hung, J. H. V. Price, N. K. Daga, N. Naz, J. Prawiharjo, D. C. Hanna, D. P. Shepherd, D. J. Richardson, J. W. Dawson, C. W. Siders, and C. P. Barty, Opt. Express **16**, 5813 (2008).

[2] V. S. Malinovsky and J. L. Krause, Phys. Rev. A **63**, 043415 (2001).

[3] J. X. Cheng and X. S. Xie, J. Phys. Chem. B **108**, 827 (2004).

[4] W. R. Browne and J. J. McGarvey, Coord. Chem. Rev. **251**, 454 (2007).

[5] R. S. Judson and H. Rabitz, Phys. Rev. Lett. **68**, 1500 (1992).

[6] S. A. Rice and M. Zhao, *Optical Control of Molecular Dynamics* (Wiley, New York, 2000).

[7] M. Shapiro and P. Brumer, *Principles of the Quantum Control of Molecular Processes* (Wiley, New York, 2003).

[8] K. Bergmann, H. Theuer, and B. W. Shore, Rev. Mod. Phys. **70**, 1003 (1998).

[9] B. J. Pearson, J. L. White, T. C. Weinacht, and P. H. Bucksbaum, Phys. Rev. A **63**, 063412 (2001).

[10] T. C. Weinacht, R. Bartels, S. Backus, P. H. Backsbaum, B. Pearson, J. M. Geremia, H. Rabitz, H. C. Kapteyn, and M. M. Murnane, Chem. Phys. Lett. **344**, 333 (2001).

[11] S. A. Malinovskaya, P. H. Bucksbaum, and P. R. Berman, Phys. Rev. A **69**, 013801 (2004).

[12] S. A. Malinovskaya, Phys. Rev. A **73**, 033416 (2006).

[13] D. Oron, N. Dudovich, D. Yelin, and Y. Silberberg, Phys. Rev. A **65**, 043408 (2002).

[14] D. Oron, N. Dudovich, D. Yelin, and Y. Silberberg, Phys. Rev. Lett. **88**, 063004 (2002).

[15] D. Romanov, A. Filin, R. Compton, and R. Levis, Opt. Lett. **32**, 3161 (2007).

[16] F. Ganikhanov, C. L. Evans, B. G. Saar, and X. S. Xie, Opt. Lett. **31**, 1872 (2006).

[17] C. L. Evans, E. O. Potma, M. Puoris'haag, D. Cté, C. P. Lin, and X. S. Xie, Proc. Natl. Acad. Sci. USA **102**, 16807 (2005).

[18] E. O. Potma, C. L. Evans, and X. S. Xie, Opt. Lett. **31**, 241 (2006); M. Jurna, J. P. Korterik, C. Otto, J. L. Herek, and H. L. Offerhaus, Opt. Express **16**, 15863 (2008).

[19] F. Lu, W. Zheng, C. Sheppard, and Z. Huang, Opt. Lett. **33**, 602 (2008).

[20] J. P. Ogilvie, E. Beaurepaire, A. Alexandrou, and M. Joffre, Opt. Lett. **31**, 480 (2006).

[21] M. Cui, M. Joffre, J. Skodack, and J. P. Ogilvie, Opt. Express **14**, 8448 (2006).

[22] S. A. Malinovskaya and V. S. Malinovsky, Opt. Lett. **32**, 707 (2007).

[23] D. DeMille, Phys. Rev. Lett. **88**, 067901 (2002).

[24] W. H. Press, S. A. Teukolsky, W. T. Vetterling, and B. P. Flannery, *Numerical Recipes in Fortran 77: The Art of Scientific Computing* (Cambridge University Press, Cambridge, 2001).

[25] T. C. Weinacht, J. L. White, and P. H. Bucksbaum, J. Phys. Chem. A **103**, 10166 (1999).

[26] M. O. Scully and M. S. Zubairy, *Quantum Optics* (Cambridge University Press, Cambridge, UK, 2002).

[27] S. A. Malinovskaya, P. H. Bucksbaum, and P. B. Berman, J. Chem. Phys. **121**, 3434 (2004).